GEOPHYSICAL RESEARCH LETTERS, VOL. 40, 4001–4006, doi:10.1002/grl.50785, 2013

Tsunami speed variations in density-stratified compressible global oceans

Shingo Watada[1]

Received 18 May 2013; revised 10 July 2013; accepted 20 July 2013; published 12 August 2013.

[1] Tsunami speed variations in the deep ocean caused by seawater density stratification is investigated using a newly developed propagator matrix method that is applicable to seawater with depth-variable sound speeds and density gradients. For a 4 km deep ocean, the total tsunami speed reduction is 0.44% compared with incompressible homogeneous seawater; two thirds of the reduction is due to elastic energy stored in the water and one third is due to water density stratification mainly by hydrostatic compression. Tsunami speeds are computed for global ocean density and sound speed profiles, and characteristic structures are discussed. Tsunami speed reductions are proportional to ocean depth with small variations, except in warm Mediterranean seas. The impacts of seawater compressibility and the elasticity effect of the solid earth on tsunami traveltime should be included for precise modeling of transoceanic tsunamis. **Citation:** Watada, S. (2013), Tsunami speed variations in density-stratified compressible global oceans, *Geophys. Res. Lett.*, *40*, 4001–4006, doi:10.1002/grl.50785.

1. Introduction

[2] Recent tsunami observations in the deep ocean, such as the Deep-ocean Assessment of Reporting of Tsunamis stations on the deep ocean floor [*Wei et al.*, 2008; *Kusumoto et al.*, 2011; *Fujii and Satake*, 2013], tsunami sensors attached to the deep ocean bottom cables, and GPS buoys continuously recording sea surface elevations [*Kato et al.*, 2011], have accumulated unequivocal evidence that tsunami traveltime delays compared with the linear long-wave tsunami simulations occur during tsunami propagation in the deep ocean. The delay is up to 2% of the tsunami traveltime.

[3] *Watada et al.* [2011, 2012] investigated the cause of the delay using the normal mode theory of tsunamis [*Ward*, 1980; *Okal*, 1982] and attributed the delay to the compressibility of seawater, the elasticity of the solid earth, and the gravitational potential change associated with mass motion during the passage of tsunamis. The normal mode theory has been applied to earth models with a compressible homogeneous ocean layer. *Okal* [1982] obtained an asymptotic formula of the effect of seawater compressibility on the tsunami propagation speed. *Tsai et al.* [2013] gave a back-of-an-envelope estimate of the tsunami speed reduction caused by the elastic solid earth and compressible seawater and found a factor inconsistency in the estimates of the effect of the seawater compressibility by *Okal* [1982] and by *Tsai et al.* [2013].

[4] Tsunami speed is affected by the seawater compressibility in two ways. The gravity potential energy of elevated and depressed seawater is not only converted to kinetic energy but also stored and released as an elastic energy in the seawater by the fluctuating hydrodynamic pressure. For a given input of gravity potential energy, smaller available tsunami kinetic energy for tsunami motion in the compressible water compared with the incompressible water results in a smaller wave frequency and hence lower tsunami speed. Real seawater is inevitably density stratified by the hydrostatic compression. The long-wave speed of a density-stratified fluid is always slower than that of a homogeneous fluid, as we see in the application section. Density stratification is also controlled by the temperature and salinity vertical profiles. The normal mode approach [e.g., *Ward*, 1980; *Okal*, 1982; *Watada et al.*, 2011, 2012] has overlooked the stratification of seawater, and *Tsai et al.* [2013] assumed an adiabatic density profile of seawater. It is desirable to discuss the compressibility effect and density stratification effect on tsunami speed separately.

[5] This paper focuses on tsunami speed reductions caused by the density stratification and the compressibility of seawater. Starting from a propagator matrix of a single-fluid layer with a constant sound speed and a density scale height, a dispersion relation of water waves is computed for a density-stratified ocean represented by a stack of thin water layers each with a constant density gradient and a sound velocity. The analytic forms of the dispersion relation for singe- and two-layer models are compared with the known dispersion relations of compressible and incompressible water cases. Finally, based on the ocean grid model of the World Ocean Atlas 2009 [*Boyer et al.*, 2009] (hereinafter WOA09), global distribution of tsunami speed perturbations and the impacts of the variability of ocean structure on the global distribution of tsunami speed perturbations are discussed.

2. Theory

[6] The equations of motion of a compressible inviscid fluid are found in e.g., section 6.14 of *Gill* [1982] and equation 2.10 of *Watada* [2009]. The x and z axes are taken along the horizontal and vertical upward positive directions, respectively. The ocean bottom is at $z = 0$. ρ, p, (u_x, u_z), (v_x, v_z) represent density, pressure, fluid displacement, and velocity, respectively, and g is constant gravity downward (Figure 1). The subscript l denotes lth layer, and the subscript o denotes the background equilibrium state, the superscript $'$

Additional supporting information may be found in the online version of this article.

[1]Earthquake Research Institute, University of Tokyo, Tokyo, Japan.

Corresponding author: S. Watada, Earthquake Research Institute, University of Tokyo, 1-1-1 Yayoi, Bunkyo-ku, Tokyo 113-0032, Japan. (watada@eri.u-tokyo.ac.jp)

0094-8276/13/10.1002/grl.50785

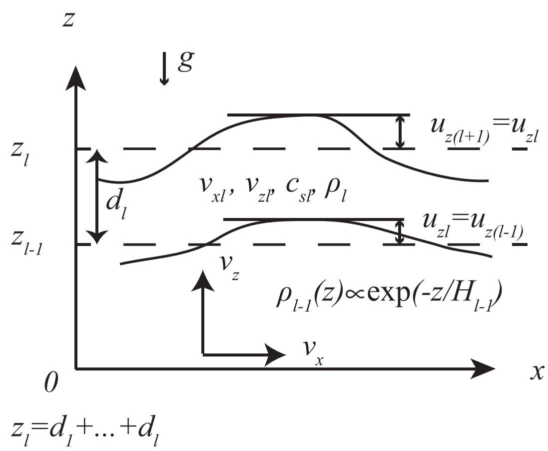

Figure 1. Multiple-layer model.

and prefix δ denote Eulerian and Lagrangian perturbations, respectively. For brevity, the subscript l is omitted when the layer is obvious and is used when needed. u, v, and the variables with $'$ and δ are assumed small, and higher order terms are neglected.

[7] Elimination of density perturbation terms in the linearized momentum equation, the mass conservation equation, and the adiabatic equation of states, and the use of the Lagrangian pressure perturbation yield the set of equations

$$\frac{\partial V_x}{\partial t} = -\frac{\partial(\delta P + gU_z)}{\partial x}, \tag{1}$$

$$\frac{\partial}{\partial t}\left(\frac{\partial}{\partial z} - \Gamma\right) V_z = \left(\frac{\partial^2}{\partial x^2} - \frac{1}{c_s^2}\frac{\partial^2}{\partial t^2}\right)(\delta P + gU_z), \tag{2}$$

$$\left(\frac{\partial^2}{\partial t^2} + N^2\right) V_z = -\frac{\partial}{\partial t}\left(\frac{\partial}{\partial z} + \Gamma\right)(\delta P + gU_z), \tag{3}$$

where the density-scaled velocities and the pressure perturbation are defined by

$$V_x = \rho_o^{0.5} v_x,\ V_z = \rho_o^{0.5} v_z,\ P = \rho_o^{-0.5} p',\ \delta P = \rho_o^{-0.5}\delta p. \tag{4}$$

U_z and V_z are related by $U_z = \int V_z \mathrm{d}t$ and $P = \delta P + gU_z$, and c_s is the sound velocity. ρ_o and c_s are dependent on z only. $\Gamma(z)$ and the buoyancy frequency $N(z)$ are defined by

$$\Gamma(z) = \frac{1}{2\rho_o}\frac{d\rho_o}{dz} + \frac{g}{c_s^2},\ N^2(z) = -g\left(\frac{1}{\rho_o}\frac{d\rho_o}{dz} + \frac{g}{c_s^2}\right). \tag{5}$$

Assuming a constant scale height $\frac{1}{H} = -\frac{1}{\rho_o}\frac{d\rho_o}{dz}$ for density and a constant c_s within the lth layer, N^2 and Γ become constant and the fluid density is expressed by

$$\rho_o(z) = \rho_{ob}\exp\left(-\frac{z}{H}\right) = \rho_{ot}\exp\left(\frac{d_l - z}{H}\right), \tag{6}$$

where the subscripts t and b denote quantities at the top and bottom of the layer, respectively, and d_l denotes the thickness of the layer. Adopting a plane wave solution for the density-scaled variables of the form $\exp(i(kx + mz - \omega t))$, the differential equations (2) and (3) are expressed by

$$E\begin{pmatrix} V_z \\ \delta P + \frac{ig}{\omega}V_z \end{pmatrix} = EF\boldsymbol{O}(z) = 0, \tag{7}$$

where

$$E = \begin{pmatrix} \omega(m + i\Gamma) & -\left(\frac{\omega^2}{c_s^2} - k^2\right) \\ (N^2 - \omega^2) & \omega(m - i\Gamma) \end{pmatrix}, \tag{8}$$

$$F = \begin{pmatrix} 1 & 0 \\ \frac{ig}{\omega} & 1 \end{pmatrix},\ \boldsymbol{O}(z) = \begin{pmatrix} V_z \\ \delta P \end{pmatrix}. \tag{9}$$

By the density scaling in equation (4), the coefficient matrices E and F are independent on z and the dispersion relation between $k, m,$ and ω is computed from $\det\|EF\| = \det\|E\|\det\|F\| = \det\|E\| = 0$. δP, P, V_x, and V_z share the dispersion relation that

$$m^2 = k^2\left(1 - \frac{\omega^2}{k^2 c_s^2}\right)\left(\frac{N^2}{\omega^2} - 1\right) - \Gamma^2. \tag{10}$$

[8] Because m^2 is a constant real number for a given (ω, k) in the lth layer, $R(z)$, the dependence of the normalized vertical velocity V_z on z satisfies the differential equation

$$\frac{d^2R}{dz^2} + m^2 R = \frac{d^2R}{dz^2} - M^2 R = 0, \tag{11}$$

where M is defined by $M^2 = -m^2$, and its solution has the form

$$V_z(x, z, t) = \rho_o^{0.5}(z) v_z(x, z, t) = R(z)\exp(i(kx - \omega t)), \tag{12}$$

$$R(z) = C\cos(mz) + D\sin(mz) = C\cos(iMz) + D\sin(iMz), \tag{13}$$

where C and D are constants to be determined from boundary conditions. Note that in the case of $m^2 < 0$, $\cos(mz)$ should be interpreted as $\cos\left(i\sqrt{-m^2}z\right) = \cosh(Mz)$ and $\sin(mz)$ as $\sin(i\sqrt{-m^2}z) = i\sinh(Mz)$.

[9] From two sets of $V_z(z)$ and $\delta P(z)$ at $z = z_{l-1}$ and z_l, C and D are eliminated and $A(d_l)$, the propagator matrix from $z = z_{l-1}$ to $z = z_l = z_{l-1} + d_l$ of a vector $\boldsymbol{o}(z)^T = (v_z(z), \delta p(z))^T$, where the superscript ^{T} denotes the transpose of a matrix, is obtained (detailed steps are in the supporting information) as

$$\begin{pmatrix} \rho_o^{-0.5}(z_l) & 0 \\ 0 & \rho_o^{0.5}(z_l) \end{pmatrix}\boldsymbol{O}(z_l) = \boldsymbol{o}(z_l) = A(d_l)\boldsymbol{o}(z_{l-1}), \tag{14}$$

where the (i,j) matrix element of matrix $A(d_l)$ is given. If $M^2 = -m^2 > 0$,

$$a_{11}(d_l) = \{\omega M c(d_l) + G s(d_l)\}/(\omega M)\exp\left(\frac{d_l}{2H_l}\right), \tag{15}$$

$$a_{12}(d_l) = is(d_l)/(q\omega M)/\rho_{ol-0.5}, \tag{16}$$

$$a_{21}(d_l) = iq(G^2 - \omega^2 M^2)s(d_l)/(\omega M)\rho_{ol-0.5}, \tag{17}$$

$$a_{22}(d_l) = \{\omega M c(d_l) - G s(d_l)\}/(\omega M)\exp\left(-\frac{d_l}{2H_l}\right), \tag{18}$$

and if $m^2 = -M^2 > 0$,

$$a_{11}(d_l) = \{\omega m f(d_l) + G e(d_l)\}/(\omega m)\exp\left(\frac{d_l}{2H_l}\right), \tag{19}$$

$$a_{12}(d_l) = ie(d_l)/(q\omega m)/\rho_{ol-0.5}, \tag{20}$$

$$a_{21}(d_l) = iq(G^2 + \omega^2 m^2)e(d_l)/(\omega m)\rho_{ol-0.5}, \tag{21}$$

$$a_{22}(d_l) = \{\omega m f(d_l) - G e(d_l)\}/(\omega m)\exp\left(-\frac{d_l}{2H_l}\right), \tag{22}$$

$1/q = \frac{\omega^2}{c_s^2} - k^2$, $G = \frac{1}{\omega}\{\omega^2\Gamma - (\frac{\omega^2}{c_s^2} - k^2)g\} = \frac{1}{\omega}\{k^2 g - \frac{\omega^2}{2H}\}$, $c(z) = \cosh(Mz)$, $s(z) = \sinh(Mz)$, $e(z) = \sin(mz)$, $f(z) = \cos(mz)$, and $\rho_{ol-0.5} = \rho_o(z = \frac{z_l + z_{l-1}}{2})$ is the water density at the midpoint of the lth layer. If the layer density is constant,

Table 1. Tsunami Speed of Single-Layer Ocean Models[a]

Case	H (km)	Cs (m/s)	N (cph)	Cp[b] (m/s)	$\frac{\Delta Vp}{Vp}$(%)	$\frac{\Delta Vp}{Vp} / \frac{\rho_b-\rho_t}{\bar{\rho}}$
A	∞	∞	0	198.214	-	-
B	∞	1500	$N^2 < 0$[c]	197.637	–0.291	–0.169
C	229.1	∞	3.75	197.926	–0.145	–0.084
D	229.1	1500	0	197.352	–0.435	–0.253

[a]Depth averaged densities are the same.
[b]Evaluated at a wavelength of 8000 km as a long-wave limit.
[c]Superadiabatic density profile which does not exist stably in nature.

factors $\exp(\pm\frac{d_l}{2H_l})$ are replaced by 1. The propagator matrix, which was also developed for the atmospheric waves by *Harkrider* [1964], has the same characteristics with $\det \|A(z)\| = 1$.

[10] Vertically non-uniform stratification of seawater is modeled as stacked multiple thin layers, each with a constant-scale height and a constant sound speed. A density jump can exist between the layers if $\rho_{ol}(z_l) \neq \rho_{ol+1}(z_l)$. In that case, δp but not p' is continuous at the boundary $z = z_l$; hence, $\boldsymbol{o}(z_l)$ is always continuous across the internal boundaries at z_l. B_L, the propagator matrix from the bottom to the top of L-stacked layers, is computed as

$$\boldsymbol{o}(z_L) = A_L(d_L)A_{L-1}(d_{L-1})\cdots A_1(d_1)\boldsymbol{o}(z_0) = B_L\boldsymbol{o}(z_0), \quad (23)$$

where z_0 and z_L are the bottom and top of L layers, respectively.

[11] The boundary conditions are $v_z(z_0) = 0$ at the rigid bottom and $\delta p(z_L) = 0$ at the free surface. Thus, the dispersion relation between the horizontal wave number k and the angular frequency ω for a given layered structure $(\rho_{obl}, H_l, c_{sl}, d_l, l = 1, \cdots, L)$ is expressed by $b_{L22}(\omega, k) = 0$, where b_{Lij} represents the (i,j) matrix element of 2×2 matrix B_L. The propagator matrix B_L is applicable to all types of linear water waves including acoustic waves, surface gravity waves, and internal gravity waves.

3. Application

3.1. Single Layer

[12] The dispersion relation of a single layer ($L = 1$) using a_{Lij}, the (i,j) matrix element of 2×2 matrix A_L, is

$$b_{122}(\omega, k) = a_{122}(\omega, k) = -\omega Mc(d) + Gs(d) = 0, \quad (24)$$

which is rewritten explicitly as

$$C_p^2(\omega, k) \equiv \frac{\omega^2}{k^2} = d\left(g - \frac{\omega^2}{2k^2H}\right)\frac{\tanh(Md)}{Md}, \quad (25)$$

where C_p is the phase velocity. The newly obtained dispersion equation (25) expresses how the density stratification and compressibility alter the dispersion relation of water waves of a single layer. Note that in a single-layer case, it is the density scale height and not the absolute density that contributes to the dispersion relation. When $M^2 < 0$, replacing M by m and tanh by tan gives the correct dispersion relation. Assuming a homogeneous ($\frac{1}{H}$=0) incompressible ($\frac{1}{c_s}$=0) single layer, $\omega^2 = gk\tanh(kd)$ is confirmed.

[13] To evaluate the effects of the density stratification and the compressibility of seawater separately, four single-layer problems, in which parameters H and c_s are constant (Table 1), are examined (Figure 2). Assuming adiabatic density stratification of compressible water, i.e., $N = 0$, the scale height is estimated as $H = c_s^2/g$. For a 4 km deep ocean with $g = 9.822$ m/s^2 and $H = 229.1$ km, the density increases by $\frac{\rho_b-\rho_t}{\bar{\rho}} = 1.72\%$ from the bottom to the top of the ocean. When the ocean layer has uniform density and a constant sound velocity (case B), the dispersion relation equation (25) reduces to

$$C_p^2(\omega, k) \equiv \frac{\omega^2}{k^2} = gd\frac{\tanh(Md)}{Md}, \quad (26)$$

where $M^2 = k^2\left(1 - \frac{\omega^2}{k^2c_s^2} + \frac{g^2}{\omega^2c_s^2}\right)$. Assuming long-wave $Md \ll 1$ and knowing that the tsunami of the Earth's ocean satisfies $\frac{\omega^2}{k^2} \ll c_s^2$, the dispersion relation for waves with horizontal wavelength $\lambda = \frac{2\pi}{k} \gg 200$ km becomes (details are in the supporting information)

$$C_p(\omega, k) \approx \sqrt{gd\left(1 - \frac{\omega^2}{3k^2c_s^2}\right)} \approx \sqrt{gd}\left(1 - \frac{gd}{6c_s^2}\right). \quad (27)$$

When water is stratified adiabatically with a uniform sound velocity (case D), gH is equal to c_s^2 and the dispersion relation equation (25) reduces to

$$C_p^2(\omega, k) \equiv \frac{\omega^2}{k^2} = gd\left(1 - \frac{\omega^2}{2k^2c_s^2}\right)\frac{\tanh(Md)}{Md}, \quad (28)$$

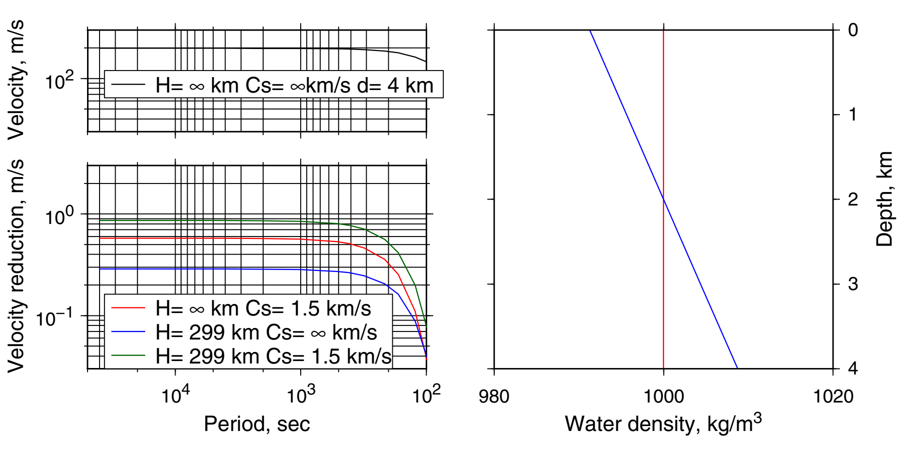

Figure 2. Dispersion curves of the surface gravity waves for the ocean structures in Table 1. (top left) Reference dispersion curve of a 4 km deep incompressible homogeneous ocean. (bottom left) Phase velocity reduction from the reference. (right) Density structure. The blue line overlaps the green line, and red line overlaps the black line.

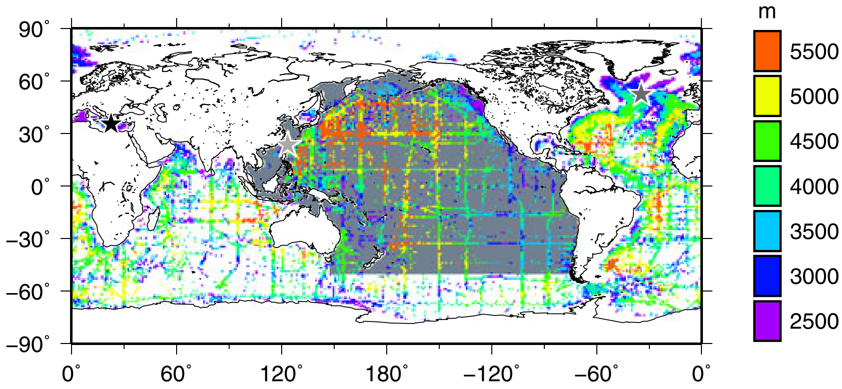

Figure 3. Data locations where a vertical ocean profile deeper than 2500 m is available in WOA09. The dark gray area indicates the Pacific Ocean defined in WOA09.

where $M^2 = k^2\left(1 - \frac{\omega^2/k^2}{c_s^2}\right) + \frac{1}{4H^2}$. Again, with the long-wave and $\frac{\omega^2}{k^2} \ll c_s^2$ assumptions, the dispersion relation for waves with horizontal wavelength $\lambda \gg 200$ km becomes (details are in the supporting information)

$$C_p(\omega, k) \approx \sqrt{gd\left(1 - \frac{\omega^2}{2k^2c_s^2}\right)} \approx \sqrt{gd}\left(1 - \frac{\rho_b - \rho_t}{4\overline{\rho}}\right). \tag{29}$$

[14] Case B is used for normal mode tsunami computation by *Ward* [1980], *Okal* [1982], and *Watada and Kanamori* [2010]. Case D is equivalent to the ocean assumed by *Tsai et al.* [2013]. The difference of the estimates of the tsunami speed dependency on the seawater sound velocity, or incompressibility, between *Okal* [1982] and *Tsai et al.* [2013] originates from the assumption of the reference density profile of the water layer. *Okal* [1982] obtained $C_p \approx \sqrt{gd}\left(1 - \frac{gd}{6c_s^2}\right)$ for a homogeneous compressible ocean and *Tsai et al.* [2013] obtained $C_p \approx \sqrt{gd}\left(1 - \frac{\rho_b - \rho_t}{4\overline{\rho}}\right)$ for an adiabatically stratified compressible ocean. Their asymptotic tsunami speed expressions are identical to mine only when the tsunami period is much larger than 1000 s or the wavelength is much longer than 200 km, which is a stronger condition than the long-wave condition $kd \ll 1$.

3.2. Two Layers

[15] The dispersion relation of a compressive fluid with two layers of different densities (L=2) is

$$b_{222}(\omega, k) = a_{221}a_{112} + a_{222}a_{122} = 0, \tag{30}$$

which is rewritten explicitly, assuming incompressible homogeneous water, as

$$\omega^2\rho_1 \frac{\coth(k(d_1 + d_2))}{\sinh(kd_1)\sinh(kd_2)}\{\omega^2 - gk\tanh(k(d_1 + d_2))\} + (\rho_1 - \rho_2)(g^2k^2 - \omega^4) = 0. \tag{31}$$

This is equivalent to equation 17 in section 231 of *Lamb* [1945]. The dispersion relation can be rewritten as

$$p^2(x)\frac{\cosh(x)}{\sinh(\beta x)\sinh((1-\beta)x)}\left\{p^2(x) - \frac{\tanh(x)}{x}\right\} + (1-\alpha)\left\{\frac{1}{x^2} - p^4(x)\right\} = 0, \tag{32}$$

where

$$x = kD,\ D = d_1 + d_2,\ p^2(x) = \frac{\omega^2}{k^2gD}, \tag{33}$$

$$\alpha = \rho_2/\rho_1,\ \beta = d_2/D = d_2/(d_1 + d_2). \tag{34}$$

Assuming long waves ($x \ll 1$), $\tanh(x)$ is approximately x, $\coth(x)$ approximately $1/x$, $\sinh(x)$ approximately x, and $\cosh(x)$ is approximately 1, equation (32) approaches

$$p^4 - p^2 + (1-\alpha)(1-\beta)\beta = 0, \tag{35}$$

which is equivalent to equation 48 in p. 219 of *Stokes* [1880] and equation 6.2.14 of *Gill* [1982] for long waves in a two-layer fluid. The solution, which corresponds to external and internal waves (+ and –, respectively), is

$$p_\pm^2 = \frac{1}{2}\left\{1 \pm \sqrt{1 - 4(1-\alpha)(1-\beta)\beta}\right\}. \tag{36}$$

In a layered fluid, usually $\alpha = \rho_2/\rho_1 \le 1$ and $1 - \alpha \ll 1$, and two long-wave modes approach

$$p_+^2 \approx 1 - (1-\alpha)(1-\beta)\beta,\ p_-^2 \approx (1-\alpha)(1-\beta)\beta. \tag{37}$$

Imamura and Imteaz [1995] obtained the external and the internal wave phase velocities which are expressed with α and β:

$$p_+^2 = 1 - (1-\alpha)\beta,\ p_-^2 = \beta\left\{1 + \alpha\frac{\beta}{1-\beta}\right\}. \tag{38}$$

Note that α and β in *Imamura and Imteaz* [1995] are defined differently from the definitions here. Equation (38) is in error, which is easily checked, for example when $\beta = 1$, the tsunami speed p_+ should be 1, not α.

3.3. Multiple Layers

[16] As tests of the code, a density-stratified incompressible layer with a scale height H (case C in Table 1) is emulated by stacked multiple homogeneous incompressible layers (case A), and a density-stratified compressible layer (case D) by stacked multiple homogeneous compressible water layers (case B). In both cases, the computed dispersion relations of 32 layers are identical to the single-layer dispersion relation within the accuracy of numerical errors (Figures are in the supporting information). In the analysis of realistic density profiles, because N^2 determined from $\frac{d\rho_o}{dz}$ is less accurate than ρ_o measurement, a staircase representation of the density gradient with many homogeneous multiple layers is preferred to a fewer thick layers with density gradients.

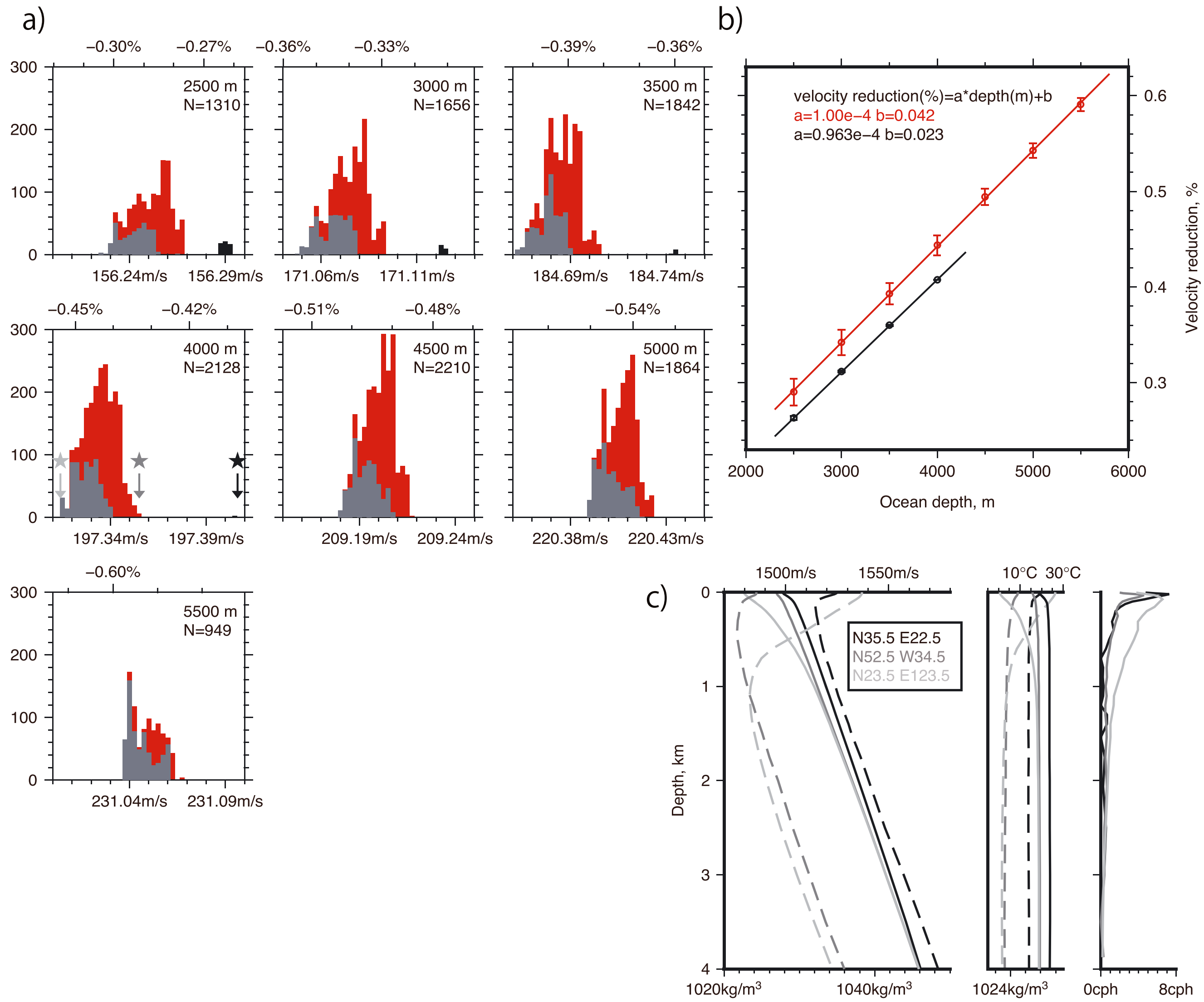

Figure 4. (a) Tsunami speed variations. Red bars represent the global speed distribution except in the Mediterranean Sea for which black bars are used. Gray bars, which are a subset of the red bars, correspond to the Pacific Ocean. Three arrows in the 4000 m histogram correspond to the stars in Figure 3. (b) Regression lines of the tsunami velocity reduction for all oceans except for the Mediterranean Sea (red line) and for the Mediterranean Sea (black line). Error bars indicate the range of the computed tsunami speed variations shown in Figure 4a. (c) Vertical ocean profiles at grid points indicated by the stars in Figure 3. Left panel shows the in situ density (solid lines) and sound velocity (dashed lines) profiles, the middle panel shows the potential density (solid lines) referenced to the surface and in situ temperature (dashed lines) profiles, and the right panel shows the buoyancy frequency profile computed from the potential density.

4. Analysis

4.1. Global Variations in Tsunami Speed Reduction

[17] Seawater density and compressibility are controlled by the pressure, salinity, and temperature of the ocean [*Talley et al.*, 2011]. WOA09 gives salinity and in situ temperature profiles at 1°× 1° time-averaged grid points. The TEOS-10 toolbox [*McDougall and Barker*, 2011] converts a WOA09 profile to in situ density and sound velocity profiles. WOA09 unevenly covers all the oceans (Figure 3). WOA09 defines 33 depth grids; the grid spacing becomes coarser with depth (every 500 m after 2000 m) toward the deepest grid at 5500 m. Local ocean models are artificially truncated at the maximum grid depth where salinity and temperature data are listed in WOA09 and do not represent the ocean profiles down to the real bottom. Tsunami speed, defined as the phase velocity at a wavelength of 8000 km in the dispersion curve, has been computed at each surface grid having a depth profile deeper than 2500 m (Figure 4c). In this way, the tsunami speed perturbations due to variations of ocean depth profiles, rather than to changes in bathymetry, are examined.

[18] Equation (37) shows that tsunami speeds in oceans with warmer and deeper (up to a half of the depth) layers are slower than incompressible long-wave speed $\sqrt{gz_L}$. The Mediterranean Sea is characterized by warm water at all depths, which results in higher sound velocities and smaller tsunami speed reductions (Figures 4a and 4b). The North Atlantic near Greenland is characterized by nearly constant cold temperature over the entire water column, similar to uniform water (Figure 4c). Adiabatically stratified cold

dense water is the easiest to sink. In fact, off the coast of Greenland in the North Atlantic is the sinking point of the great ocean conveyor ocean circulation model [*Broecker*, 2010].

[19] Given that the two vertical columns have identical sound speed, tsunami speed is larger when the potential density is constant, i.e., when the buoyancy frequency is zero throughout the water column and therefore the tsunami speed is insensitive to the absolute magnitude of water density. The western Pacific Ocean near Taiwan, which is characterized by a 1 km thick warm top layer, exhibits global maximum tsunami speed reduction in 4000 m deep oceans (Figure 4a). The difference of the tsunami speeds between near Taiwan and near Greenland is due to the thick surface warm layer near Taiwan. The difference of the tsunami speeds between near Greenland and in the Mediterranean Sea is due to temperature, hence the sound speed, differences extending throughout the water columns (Figure 4c).

5. Discussion and Conclusion

[20] The analytic forms of the dispersion relation for single- and two-layer models are compared with the known dispersion relations for compressible and incompressible water. The dispersion relation of water waves for an ocean layer found in sections 54–57 of *Eckart* [1960], which is obtained under the condition of $\Gamma = 0$ in equation (10), is extended to $\Gamma \neq 0$ and multiple-layer cases. *Panza et al.* [2000] gave a propagator matrix for seawater composed of homogeneous layers. For a 4 km deep compressible stratified ocean model, the total tsunami speed reduction is expected to be 0.44% from the tsunami speed in incompressible homogeneous seawater; 0.29% is due to the elastic energy stored in compressible water, and 0.15% is due to the density stratification mainly by the hydrostatic compression. Note that the differences in the phase velocity reduction between compressible and incompressible models are evidenced in a slight difference of the corner periods of the dispersion curves (Figure 2, bottom left).

[21] The propagator matrix method has been applied to the real ocean profiles deeper than 2500 m compiled in WOA09, and tsunami speeds in the deep oceans have been computed. An expression for the tsunami speed reduction of a given depth has been obtained as $\Delta V/V = a$*(depth, m) + b (Figure 4b), where $a = 1.00 \times 10^{-6}$ m^{-1} for an average 4000 m deep ocean (except in the Mediterranean Sea), and $a = 9.63 \times 10^{-7}$ m^{-1} for the Mediterranean Sea. The depth coefficient a has been previously estimated by *Okal* [1982] as $\frac{g}{6c_s^2} = 7.28 \times 10^{-7}$ m^{-1} and by *Tsai et al.* [2013] as $\frac{\rho_b - \rho_t}{4\bar{\rho} z_L} = 1.08 \times 10^{-6}$ m^{-1}. In the deep ocean, the tsunami speed perturbation from the average tsunami speed due to natural variations in the vertical structure of the ocean is usually ±0.01%. An exceptionally diminished tsunami speed reduction of –0.05%, i.e., faster than the global average, is found in the warm Mediterranean seas.

[22] Seawater compressibility affects tsunami speeds through its effects on density stratification and elastic energy stored in seawater. These effects, in addition to the solid earth elasticity effect and the gravitational potential perturbation effect [*Watada et al.*, 2011, 2012], should be included for the precise estimates of the traveltime of transoceanic tsunamis. Local variations in the seawater properties of deep ocean water have negligible impacts on tsunami speeds, and their effects are not likely to be observed.

[23] **Acknowledgment.** The Editor thanks Victor Tsai and an anonymous reviewer for assistance in evaluating this manuscript.

References

Boyer, T. P., et al. (2009), *World Ocean Database 2009,* S. Levitus (ed), NOAA Atlas NESDIS 66, U.S. Gov. Printing Office, Wash. D.C., 216 pp., DVDs.

Broecker, W. (2010), *The Great Ocean Conveyer*, Princeton Univ. Press, Princeton.

Eckart, C. (1960), *Hydrodynamics of Oceans and Atmospheres*, Pergamon Press, New York.

Fujii, Y., and K. Satake (2013), Slip distribution and seismic moment of the 2010 and 1960 Chilean earthquakes inferred from tsunami waveforms and coastal geodetic data, *Pure Appl. Geophys.,* doi:10.1007/s00024-012-0524-2, in press.

Gill, A. E. (1982), *Atmosphere-Ocean Dynamics*, Academic Press, New York.

Harkrider, D. G. (1964), Theoretical and observed acoustic-gravity waves from explosive sources in the atmosphere, *J. Geophys. Res.*, *69*, 5295–5321.

Imamura, F., and A. Imteaz (1995), Long waves in two layers: Governing equations and numerical model, *Sci. Tsun. Haz.*, *13*, 3–24.

Kato, T., Y. Terada, H. Nishimura, T. Nagai, and S. Koshimura (2011), Tsunami records due to the 2010 Chile Earthquake observed by GPS buoys established along the Pacific coast of Japan, *Earth Planets Space*, *63*(6), E5–E8, doi:10.5047/eps.2011.05.001.

Kusumoto, S., T. Ueno, S. Murotani, H. Tsuruoka, and K. Satake (2011), Travel time difference between observed and modeled tsunami waveform across the Pacific Ocean, Abstract presented at the 2011 Seismological Society of Japan Meeting, Shizuoka, 2–77.

Lamb, H. (1945), *Hydrodynamics*, Dover, New York.

McDougall, T. J., and P. M. Barker, (2011), Getting started with TEOS-10 and the Gibbs Seawater (GSW) Oceanographic Toolbox, *SCOR/IAPSO WG127*, 28pp., ISBN 978-0-646-55621-5.

Okal, E. A. (1982), Mode-wave equivalence and other asymptotic problems in tsunami theory, *Phys. Earth Planet. Inter.*, *30*, 1–11.

Panza, G. F., F. Romanelli, and T. B. Yanovskaya (2000), Synthetic tsunami mareograms for realistic oceanic models, *Geophys. J. Int.*, *141*, 498–508.

Stokes, G. G. (1880), On the theory of oscillatory waves, in *Math. Phys. Pap., 1*, edited by G. G. Stokes, At the University Press, Cambridge.

Tsai, V. C., J.-P. Ampuero, H. Kanamori, and D. J. Stevenson (2013), Estimating the effect of Earth elasticity and variable water density on tsunami speeds, *Geophys. Res. Lett.*, *40*, 492–496, doi:10.1002/grl.50147.

Talley, L. D., G. L. Pickard, W. J. Emery, and J. H. Swift (2011), *Descriptive Physical Oceanography: An Introduction,* 6th edn., Academic Press, London.

Ward, S. N. (1980), Relationships of tsunami generation and an earthquake source, *J. Phys. Earth*, *28*, 441–474.

Watada, S. (2009), Radiation of acoustic and gravity waves and propagation of boundary waves in the stratified fluid from a time-varying bottom boundary, *J. Fluid Mech.*, *627*, 361–377, doi:10.1017/S0022112009005953.

Watada, S., and H. Kanamori (2010), Acoustic resonant oscillations between the atmosphere and the solid earth during the 1991 Mt. Pinatubo eruption, *J. Geophys. Res.*, *115*, B12319, doi:10.1029/2010JB007747.

Watada, S., K. Satake, and Y. Fujii (2011), Origin of traveltime anomalies of distant tsunami, Abstract NH11A-1363 presented at 2011 Fall Meeting, AGU, San Francisco, Calif., 5–9 Dec.

Watada, S., S. Kusumoto, and K. Satake (2012), Cause of delayed first peak and reversed initial phase of distant tsunami, Abstract NH43B-1649 presented at 2012 Fall Meeting, AGU, San Francisco, Calif., 3–7 Dec.

Wei, Y., E. N. Bernard, L. Tang, R. Weiss, V. V. Titov, C. Moore, M. Spillane, M. Hopkins, and U. Kanoglu (2008), Real-time experimental forecast of the Peruvian tsunami of August 2007 for U.S. coastlines, *Geophys. Res. Lett.*, *35*, L04609, doi:10.1029/2007GL032250.